PCCP

RSC Publishing

PAPER

On the role of electron–nucleus contact and microwave saturation in thermal mixing DNP

Cite this: *Phys. Chem. Chem. Phys.*, 2013, **15**, 8416

Sonia Colombo Serra,*[a] Alberto Rosso[b] and Fabio Tedoldi[a]

We have explored the manifold physical scenarios emerging from a model of Dynamic Nuclear Polarization (DNP) *via* thermal mixing under the hypothesis of highly effective electron–electron interaction. When the electron and nuclear reservoirs are also assumed to be in strong thermal contact and the microwave irradiation saturates the target electron transition, the enhancement of the nuclear polarization is expected to be considerably high even if the irradiation frequency is set far away from the centre of the ESR line (as already predicted by Borghini) and the typical polarization time is reduced on moving towards the boundaries of the said line. More reasonable behaviours are obtained by reducing the level of microwave saturation or the contact between electrons and nuclei in the presence of nuclear leakage. In both cases the function describing the dependency of the steady state nuclear polarization on the frequency of irradiation becomes sharper at the edges and the build up rate decreases on moving off-resonance. Although qualitatively similar in terms of the effects produced on nuclear polarization, the degree of microwave saturation and of electron–nucleus contact has a totally different impact on electron polarization, which is of course strongly correlated to the effectiveness of saturation and almost insensitive, at the steady state, to the magnitude of the interactions between the two spin reservoirs. The likelihood of different scenarios is discussed in the light of the experimental data currently available in the literature, to point out which aspects are suitably accounted for and which are not by the declination of thermal mixing DNP considered here.

Received 24th December 2012,
Accepted 31st March 2013

DOI: 10.1039/c3cp44667k

www.rsc.org/pccp

I. Introduction

In the last decade Dynamic Nuclear Polarization (DNP) has established itself as a powerful technique to overcome the limited sensitivity of Nuclear Magnetic Resonance (NMR).[1] More recently, as a consequence of the impressive experimental results obtained over a wide area of applications, ranging from analytical[2,3] to potentially diagnostic methods,[4–6] the scientific community has started to deepen the existing theoretical knowledge about the physics of the polarization process.[7–9] Depending on the specific conditions of the experiment, the transfer of magnetic order from the electron to the nuclear system occurs by different mechanisms, namely the solid effect,[10,11] cross effect[12–15] and thermal mixing.[11,16,17] The latter regime is believed to apply to those samples and experimental conditions typically exploited in biomedical applications,[18] which nowadays are attracting great interest.

The original theoretical description of low temperature DNP *via* thermal mixing (TM) was provided by Borghini[16] and re-proposed in a slightly different fashion by Abragam and Goldman in their famous review.[11] The model is based on the hypothesis of (i) very efficient spectral diffusion, (ii) complete saturation of the irradiated Electron Spin Resonance (ESR) isocromate and (iii) the existence of a perfect contact between electrons and nuclei. The latter forces the establishment of a common temperature between nuclear and electron reservoirs at any time.

Despite the Borghini prediction qualitatively depicting some aspects of the experimental scenario, no information about the dynamics of the process is given, while the steady state nuclear polarization is always overestimated. The quantitative agreement is especially poor when moving from the centre to the edges of the ESR spectrum. In order to reduce the discrepancies between theory and experimental observations in the nuclear steady state behaviour, Jannin *et al.*[19] have recently proposed a variant of the Borghini model where the irradiated ESR line portion is only partially saturated. Again, the dynamical problem has not been tackled.

A general methodology to compute the full time evolution of the nuclear polarization in the low temperature TM regime, relying on a mean field approach and based on a proper system

[a] *Centro Ricerche Bracco, Bracco Imaging Spa, via Ribes 5, 10010 Colleretto Giacosa, TO, Italy. E-mail: sonia.colombo@bracco.com*
[b] *Université Paris-Sud, CNRS, LPTMS, UMR 8626, Orsay F-91405, France*

of rate equations, has been described in ref. 20. In this work we exploited that mathematical treatment (briefly recalled in Section II) for providing a comprehensive picture of the electron and nuclear polarization dynamics (including the relevant steady states), over the whole microwave spectrum, for different choices of the five time constants describing the basic interactions and relaxation mechanisms. In particular, under the assumption of an optimal electron spin–spin contact, the role of microwave power and electron–nucleus interaction was investigated.

The numerical results presented in Section III point out how the hypothesis of partial saturation introduced in ref. 19 not only improves the agreement between TM theory and the experimental data of steady state nuclear polarization but also predicts a more realistic behaviour for the frequency dependence of the nuclear build up time. A similar qualitative agreement is obtained by maintaining the full saturation assumption included in the original Borghini model and relaxing the constraint of perfect electron–nucleus contact, in the presence of a weak, electron independent, nuclear spin–lattice relaxation term. The two options considered, both fairly good in accounting for the behaviour of the nuclear reservoir, generate a completely different scenario in respect of the electron polarization, as widely discussed in Section IV in the light also of the experimental observations available in the literature.

In order to make the reading of the manuscript more fluent, three Appendices collecting most of the relevant mathematics have been added at the end of the main text.

II. Model overview

A system of N_n nuclear spin $\boldsymbol{I}$ ($I = 1/2$, Larmor frequency ω_n) and N_e electron spin $\boldsymbol{S}$ ($I = 1/2$, mean Larmor frequency ω_e ($\approx 10^3\omega_n$)) is considered. The electron frequency distribution (ESR line) is supposed to be inhomogeneously broadened[21] and can be conveniently decomposed into a sequence of N_p narrow individual spin packets of frequency $\omega_i = \omega_e - \Delta_i$, width $\delta\omega$ and relative weight f_i such that $\sum f_i = 1$ and $\sum f_i\Delta_i = 0$. The system is assumed to be ruled by five processes: microwave irradiation (with a characteristic time T_{1MW}), spectral diffusion (T_{2e}), ISS process (T_{ISS}), electron spin–lattice relaxation (T_{1e}) and nuclear spin–lattice relaxation (T_{1n}) (see ref. 20 for detailed description). The rate $1/T_{ISS}$ describes, as an effective parameter, both the nuclear spin diffusion process and the interaction of two generic electrons belonging to packets i and $i + \delta n_p$ (δn_p being the number of packets corresponding to ω_n) and a generic nucleus n. Electrons of the same packet are set identical by definition and characterized by a local polarization $P_{e,i}$, whereas a unique polarization P_n and inverse temperature β_n are assigned to the whole nuclear system:

$$P_n(t) = \tanh[\beta_n(t)\delta n_p]. \quad (1)$$

The system so defined is studied in the TM regime, where the spectral diffusion processes, mediated by the electron dipolar interaction, are far more efficient than any other process ($T_{2e} \to 0$). In this limit, even when the system is out of equilibrium because of the MW irradiation, a unique spin temperature is established at all times among the electron packets (Appendix A). The electron polarization $P_{e,i}(t)$ can thus be written as:

$$P_{e,i}(t) = \tanh[\beta_e(t)(\Delta_i - c(t))], \quad (2)$$

where $c(t)$ and the unique inverse temperature $\beta_e(t)$ are time-dependent parameters.

The dynamics of $P_{e,i}(t)$ and consequently of $P_n(t)$ is determined not only by the highly efficient spectral diffusion but also by the remaining four processes. Their effect is described by the system of rate equations introduced in ref. 20 and here reported for convenience of the reader (under the assumption of finite rates for all the four processes).

$$\begin{aligned}\frac{dP_{e,i}(t)}{dt} &= \frac{P_0 - P_{e,i}(t)}{T_{1e}} - \delta_{i,i_0}\frac{P_{e,0}(t)}{T_{1MW}} \\ &\quad + \frac{f_{i-\delta n_p}\Pi_- + f_{i+\delta n_p}\Pi_+}{2T_{ISS}} \\ \frac{dP_n(t)}{dt} &= \frac{P_{0n} - P_n(t)}{T_{1n}} - \frac{N_e}{2T_{ISS}N_n}\sum f_i f_{i+\delta n_p}\Pi_n\end{aligned} \quad (3)$$

where δ_{i,i_0} is a Kronecker delta and $\Pi_- = \Pi_-(i,t)$, $\Pi_+ = \Pi_+(i,t)$, $\Pi_n = \Pi_n(i,t)$ are given by the expressions:

$$\begin{aligned}\Pi_- &= P_{e,i-\delta n_p}(t) - P_{e,i}(t) - P_n(t)[1 - P_{e,i-\delta n_p}(t)P_{e,i}(t)] \\ \Pi_+ = \Pi_n &= P_{e,i+\delta n_p}(t) - P_{e,i}(t) + P_n(t)[1 - P_{e,i+\delta n_p}(t)P_{e,i}(t)]\end{aligned} \quad (4)$$

For numerical computation a discrete time step dt is introduced:

$$dt = \frac{1}{W_{1MW} + W_{ISS} + W_e + W_n}, \quad (5)$$

where $W_{1MW} = N_e f_0/T_{1MW}$, $W_e = N_e/T_{1e}$, $W_{ISS} = N_e\sum f_i f_{i+\delta n_p}/T_{ISS}$ and $W_n = N_n/T_{1n}$. After each elementary evolution step according to eqn (3), the effect of spectral diffusion (acting on a typical time scale $\delta t \approx T_{2e} < dt$) is accounted for by imposing the conditions that the polarizations $P_{e,i}(t + \delta t)$ satisfy eqn (2) and the conservation of the energy and total polarization:

$$\begin{aligned}\sum f_i[P_{e,i}(t + \delta t) - P_{e,i}(t)] &= 0 \\ \sum f_i\Delta_i[P_{e,i}(t + \delta t) - P_{e,i}(t)] &= 0\end{aligned} \quad (6)$$

In this work we investigate three distinct regimes where, in addition to spectral diffusion, one or two more processes are assumed infinitely efficient.

A. Regime I ('Borghini')

The evolution of the system is derived under the following assumptions:

- $T_{ISS} \to 0$: a perfect contact between the electron and the nuclear reservoirs which allows us to establish a common electron–nucleus inverse temperature $\beta(t) = \beta_e(t) = \beta_n(t)$ at all times (see Appendix A);
- $T_{1MW} \to 0$: a full saturation of the irradiated packet i_0 which corresponds to the assumption $P_{e,0}(t) = 0$, so that $c(t) = \Delta_0$.

The steady state solution $P_{e,i}(t \to \infty)$ and $P_n(t \to \infty)$ can be computed by solving numerically the known Borghini relation:

$$\sum f_i(\Delta_i - \Delta_0)P_{e,i} + \Delta_0 P_0 - \omega_n \frac{N_n T_{1e}}{N_e T_{1n}} P_n = 0, \qquad (7)$$

which can be easily obtained by solving the system of equations describing the time evolution of the two energy reservoirs (Zeeman electron and non-Zeeman plus Zeeman nuclear contributions, reported in eqn (c4) of ref. 20) at the steady state, under the condition $c = \Delta_0$.

The dynamics of electron and nuclear polarizations can be obtained from the system of rate equations (eqn (3)), conveniently adapted to this regime (Appendix B1). Moreover, it is possible to write the rate equation for the inverse temperature $\beta(t)$ (Appendix B1), whose solution is not an exponential function.

B. Regime II ('partial MW saturation')

The evolution of the system is derived under the following assumptions:

- $T_{ISS} \to 0$: a perfect contact between the electron and the nuclear reservoirs which imposes, as in regime I, $\beta(t) = \beta_e(t) = \beta_n(t)$;
- $T_{1MW} \neq 0$: an incomplete saturation of the irradiated packet i_0.

The steady state solution is now a function of two variables β and c and can be evaluated by numerically solving the following system of two equations:

$$\sum f_i \frac{P_0 - P_{e,i}}{T_{1e}} - f_0 \frac{P_{e,0}}{T_{1MW}} = 0$$

$$\sum \Delta_i f_i \frac{P_{e,i}}{T_{1e}} + f_0 \Delta_0 \frac{P_{e,0}}{T_{1MW}} - \frac{N_n}{N_e} \hbar \omega_n \frac{P_n}{T_{1n}} = 0 \qquad (8)$$

which is a generalized version of the Borghini relation, again obtained as steady state solution of the system of rate equations reported in eqn (c4) of ref. 20.

The evolution of $P_{e,i}(t)$ and $P_n(t)$ can be estimated by means of the system of rate equations (eqn (3)) adapted for this regime (Appendix B2).

C. Regime III (poor electron–nucleus contact)

The evolution of the system is derived under the following assumptions:

- $T_{1MW} \to 0$: a full saturation of the irradiated packet i_0 which imposes $c = \Delta_0$;
- $T_{ISS} \neq 0$: a poor contact between the electron and the nuclear reservoirs, modulated by the corresponding parameter $1/T_{ISS}$, which leads (in the presence of leakage) to two different inverse temperatures for electrons and nuclei, *i.e.* $\beta_e(t) \neq \beta_n(t)$.

The steady state solution is now a function of two variables β_e and β_n and can be evaluated by numerically solving a system composed by the Borghini relation (eqn (7), which holds also in this regime, but it is not sufficient to determine unambiguously β_e and β_n) and the rate equation for $P_n(t)$. The latter, by imposing the stationary condition, is written as:

$$P_n = \frac{\frac{N_e}{2T_{ISS}N_n}\sum f_i f_{i+\delta n_p}\left(P_{e,i} - P_{e,i+\delta n_p}\right) + \frac{P_{0n}}{T_{1n}}}{\frac{N_e}{2T_{ISS}N_n}\sum f_i f_{i+\delta n_p}\left(1 - P_{e,i}P_{e,i+\delta n_p}\right) + \frac{1}{T_{1n}}} \qquad (9)$$

The solution for $P_{e,i}(t)$ and $P_n(t)$ can be obtained from the system of rate equations (eqn (3)), conveniently adapted for this regime (Appendix B3).

In the limit $T_{ISS} \gg T_{1e}$, the contact between the electrons and the lattice is more efficient than the contact between electrons and nuclei. The steady state polarization profile $P_{e,i}$ is then achieved in a typical time of the order of T_{1e} independently from any feature of the nuclear reservoir. As a consequence, the nuclear system 'sees', through T_{ISS}, an electron thermal bath at constant temperature and the rate equation for $P_n(t)$ assumes the linear form:

$$P_n'(t) = A - BP_n(t) \qquad (10)$$

where A and B are constant terms defined as:

$$A = -\frac{N_e}{2T_{ISS}N_n}\sum f_i f_{i+\delta n_p}\left(P_{e,i+\delta n_p} - P_{e,i}\right) + \frac{P_{0n}}{T_{1n}}$$

$$B = \frac{N_e}{2T_{ISS}N_n}\sum f_i f_{i+\delta n_p}\left(1 - P_{e,i+\delta n_p}P_{e,i}\right) + \frac{1}{T_{1n}}$$

$P_{e,i}$ being given by the Borghini relation (eqn (7) in the absence of nuclei). Its solution:

$$P_n(t) = \frac{A}{B}[1 - \exp(-Bt)] \qquad (11)$$

is an exponential function with a steady state $P_n = A/B$ and an exponential time constant equal to $1/B$.

III. Numerical results

The three regimes introduced in Section II have been explored by computing a set of build up curves (*i.e.* polarization *versus* time) for different values of the significant parameters: i_0, T_{1MW}, T_{ISS} and T_{1n}. All the other parameters of the rate equations, when not differently stated, have been set as follows: $N_n/N_e = 1000$, $T_{1e} = 1$ s, $N_p = 15$, $\delta n_p = 3$ and f_i defined according to a Gaussian function with a full width at half maximum $\Delta\omega_e = 63$ MHz and truncated at 3σ. This set of parameters is chosen to represent a sample of [1-13C]-pyruvic acid doped with the 15 mM trityl radical in a magnetic field $B_0 = 3.35$ T, at temperature $T = 1.2$ K. Such a well known mixture is an ideal prototype to be tested against the outcome of our calculations, since it was argued to polarize *via* TM[18] and has been studied experimentally in great detail.[18,22,23] The build up curves obtained from the numerical simulation have been fitted by the phenomenological law:

$$P(t) = P_0[1 - \exp(-t/T_{pol})^{\alpha}] \qquad (12)$$

where P_0 is the steady state value of the polarization, T_{pol} is the polarization time and α is a stretching exponent. For $\alpha = 1$, the usual exponential function is recovered.

A. Regime I: the Borghini model

The physical scenario emerging under the assumptions defining the regime I is summarized in Fig. 1. Panel A shows the steady state nuclear polarization P_n as a function of the microwave frequency ω_{MW} in the absence of leakage and when T_{1n} = 10 000 s. The same curve is obtained by solving eqn (7). The calculated values are generally higher than those experimentally observed especially when moving from the centre to the edges of the ESR line. A maximum nuclear polarization of 0.85 is reached in the absence of leakage when the microwave frequency is set to $\omega_{MW,opt} = \omega_e - 43$ MHz (corresponding to the irradiation of the packet $i_0 = 4$). Leakage has only a moderate effect on the curve, leading to a 13% reduction in the maximum polarization level for T_{1n} = 10 000 s.

Another interesting quantity for comparison with experiments (see Section IV) is the average electron polarization $\langle P_e(t)\rangle$, defined as:

$$\langle P_e(t)\rangle = \sum f_i P_{e,i}(t) \quad (13)$$

The steady state value $\langle P_e\rangle$ of this quantity is reported in panel B of Fig. 1. When the irradiation frequency ω_{MW} is close to ω_e, the ESR line is effectively saturated, *i.e.* $\langle P_e\rangle \approx 0$. Conversely when the irradiation frequency is set at the edges of the ESR line, $\langle P_e\rangle \rightarrow P_0$ because of the low weight f_i of the side packets.

The dynamical evolution of the spin systems can be derived by means of eqn (B2) and (B1). The behaviour of the nuclear polarization time as a function of ω_{MW} is shown in Fig. 1, panel C.

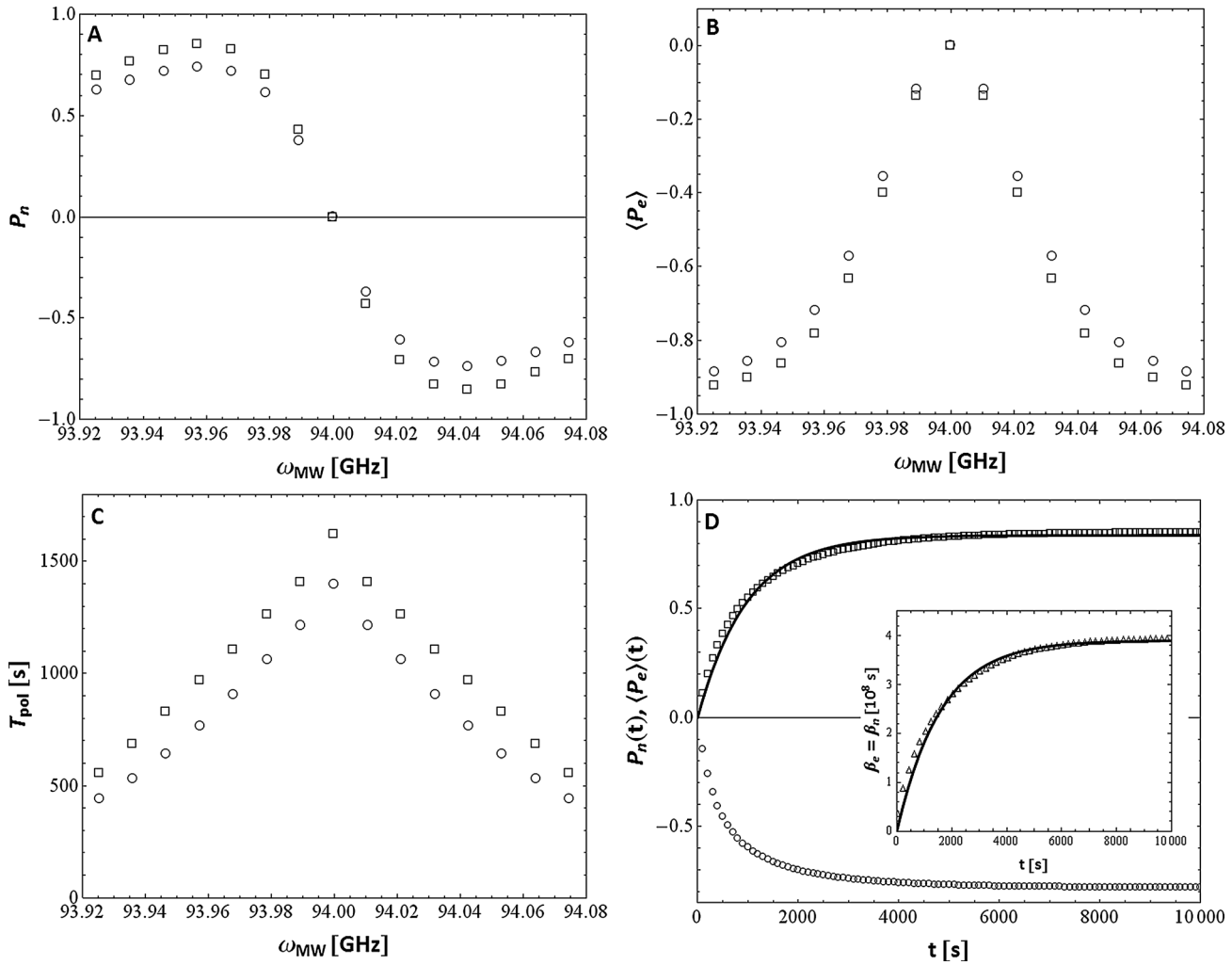

Fig. 1 Overview of nuclear and electron polarization in TM-DNP under the assumption defining regime I (T_{2e} = 0 s, T_{ISS} = 0 s, T_{1MW} = 0 s) at 3.35 T and 1.2 K. The nuclei/electrons ratio has been set to N_n/N_e = 1000, whereas the electron longitudinal relaxation time is assumed to be T_{1e} = 1 s. Panel A: steady state nuclear polarization P_n as a function of the irradiating frequency ω_{MW} in the absence of leakage (squares) and with T_{1n} = 10 000 s (circles). Panel B: average electron polarization $\langle P_e\rangle$ as a function of ω_{MW} in the absence of leakage (squares) and with T_{1n} = 10 000 s (circles). Panel C: nuclear polarization time T_{pol} as a function of ω_{MW} in the absence of leakage (squares) and with T_{1n} = 10 000 s (circles). Panel D: nuclear and average electron polarization build up curves $P_n(t)$ (squares) and $\langle P_e(t)\rangle$ (circles) at $\omega_{MW,opt}$ in the absence of leakage. The growing curve of the inverse temperature $\beta(t)$ (triangles) is represented in the inset. The non-linearity of the differential equations which regulate this regime is reflected in the lack of agreement between the calculated trend of $P_n(t)$ and $\beta(t)$ and the exponential best fittings (solid lines).

The larger is the shift between ω_e and ω_{MW}, the shorter is T_{pol} or, in other words, the steady state is achieved faster when the edges of the ESR line are irradiated.

Finally, in panel D of Fig. 1 the nuclear and electron build up curves are displayed for $\omega_{MW,opt}$ (*i.e.* with $i_0 = 4$) in the absence of leakage starting from the thermal Boltzmann equilibrium condition $P_n \approx 0$ and $P_{e,i} = P_0$, $\forall i$. As introduced in the previous section, the same inverse temperature $\beta(t)$ (see inset) characterizes both nuclear and electron reservoirs. The dynamics is non-exponential as can be noticed by the mismatch between the best fitting curve and the simulated data if a stretching exponential $\alpha = 1$ is assumed. The function describing the dynamics of $\beta(t)$ is computed in Appendix B1. Despite nuclei and electrons share the same temperature over time, since the hyperbolic tangent is a non-linear function, the nuclear and electron polarization build up times are slightly different, although both in the order of 10^3 s. The initial condition $\beta(t = 0) \approx 0$ originates as follows:

- when MW is switched on the packet i_0 is immediately saturated ($P_{e,0} = 0$) due to the assumption $T_{1MW} \to 0$;
- the fast spectral diffusion ($T_{2e} \to 0$) imposes: $P_{e,i}(t = 0) = \tanh[\beta(t = 0)(\Delta_i - \Delta_0)]$;
- the effective contact between electrons and nuclei gives: $\beta(t = 0) = \beta_n(t = 0) \approx 0$.

B. Regime II: partial MW saturation

An overview of the regime characterized by a partial saturation of the ESR line is presented in Fig. 2. In panels A and B, P_n and $\langle P_e \rangle$ as a function of ω_{MW} are shown for $T_{1MW} = 0$, 0.1 and 1 s, *i.e.* moving from high to low MW power. The effect of a partial saturation is twofold: on one side a significant reduction of the maximum nuclear and electron polarization values is observed.

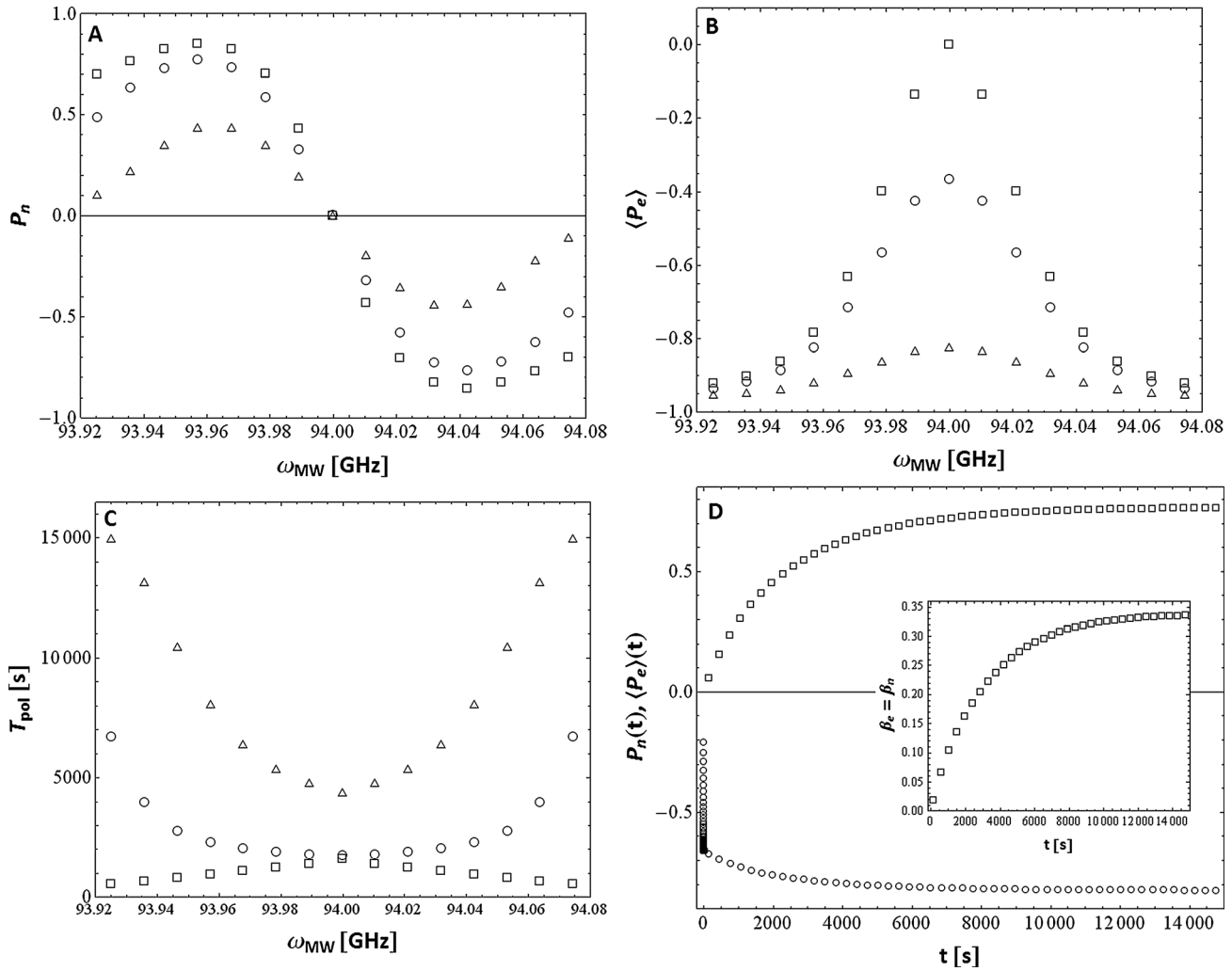

Fig. 2 Overview of nuclear and electron polarization in TM-DNP under the assumption defining regime II ($T_{2e} = 0$ s, $T_{ISS} = 0$ s, $T_{1MW} \neq 0$) at 3.35 T and 1.2 K, with $N_n/N_e = 1000$, $T_{1e} = 1$ s and in the absence of leakage. Panel A: steady state nuclear polarization P_n as a function of the irradiating frequency ω_{MW} with $T_{1MW} = 0$ (squares), 0.1 s (circles) and 1 s (triangles). Panel B: average electron polarization $\langle P_e \rangle$ as a function of ω_{MW} with $T_{1MW} = 0$ (squares), 0.1 s (circles) and 1 s (triangles). Panel C: nuclear polarization time T_{pol} as a function of ω_{MW} with $T_{1MW} = 0$ (squares), 0.1 s (circles) and 1 s (triangles). Panel D: nuclear polarization build up curve $P_n(t)$ for $T_{1MW} = 0.1$ s at $\omega_{MW,opt}$. The mismatch between numerical data and exponential best fitting (solid line) points out the non-linearity of the phenomenon. The inset shows the corresponding growth of the inverse temperature $\beta(t)$.

On the other side a clipping of the wings of the steady state nuclear polarization curve occurs, making the latter more similar to the DNP spectrum experimentally observed in the prototype trityl doped sample studied in ref. 18. That incomplete MW saturation can be invoked to better account for nuclear steady state data was pointed out previously in ref. 19. Thanks to this assumption the authors succeeded in fitting the DNP spectrum of a [1-13C]-sodium acetate sample doped with TEMPO, a free radical characterized by a much shorter T_{1e} with respect to trityls and by a higher anisotropy of the *g*-tensor, resulting in turn in a wider ESR spectrum ($\approx$200 MHz *vs.* 60 MHz of trityls).

The behaviour of the polarization time *versus* ω_{MW} (panel C) is, interestingly, completely different from regime I. As long as the irradiation frequency is close to ω_e, T_{pol} is relatively short, becoming longer and longer on moving towards the edges of the ESR line (from 1800 to 6800 s when T_{1MW} = 0.1 s and from 4800 to 15 000 s when T_{1MW} = 1 s). As expected, longer is T_{1MW}, less effective the polarization mechanism is.

The time evolution of P_n represented in panel D as well as the build up curve of β (inset) are similar to those obtained in regime I, with a non-exponential behaviour (a rigorous demonstration is not reported in this case) and a typical time constant in the order of 10^3 s. The build up of the electron polarization instead is somehow more complex and characterized by two different time scales. The details of such behaviour are analyzed in Appendix C.

C. Regime III: poor electron–nucleus contact

The third regime is characterized by a finite contact rate between nuclei and electrons. Nuclear and electron polarization were computed for T_{ISS} = 0.1 and 1 s both in the absence of leakage and with T_{1n} = 10 000 s. The main results are shown in Fig. 3, following the same scheme of the regimes discussed above. Panel A shows the dependence of the nuclear polarization on ω_{MW}. In the absence of leakage, as already discussed in ref. 20, the contact rate T_{ISS} does not affect the steady state but only the dynamics and thus the two curves at different T_{ISS} overlap. In the presence of leakage P_n is reduced. The longer is T_{ISS} the higher the decrease is. Moreover, the reduction is more significant at the edges of the DNP spectrum, a behaviour that becomes clear in the light of panel C, where T_{pol} is shown to be strongly increased at the wings of the spectrum. As a consequence, nuclear relaxation (with rate T_{1n} = 10 000 s) becomes a strong competing mechanism with respect to the ISS process, forcing P_n towards a lower steady state value.

Panel B highlights a rather interesting feature of regime III: the steady state electron polarization is almost unaffected either by T_{ISS} and T_{1n}. This indicates that the nuclear system, for sufficiently high values of T_{ISS}, is only a spectator of the electrons re-arrangement under MW irradiation, playing no active roles in the evolution of the electron systems towards their equilibrium. Evolution that proceeds through a two-step process is discussed in Appendix C. Nuclei have a 'delayed response' characterized by a time constant in the order of $N_n/(N_e T_{ISS})$ (about 10^4–10^5 s for the set of parameters used here) and by an exponential shape as confirmed by the good match between the fitting and the simulated data in panel D and demonstrated in Section II. The exponential time course of $P_n(t)$ stems from the linear rate equation (eqn (10)) that further remarks the passive role of the nuclear reservoir in the polarization process of electrons. Correspondingly the nuclear inverse temperature $\beta_n(t)$ builds up (inset of panel D) towards a steady state value that, in the presence of leakage, is substantially different from the end value of $\beta_e(t)$. One has, for instance, $\beta_n = 1.84 \times 10^8$ s *vs.* $\beta_e(t) = 3 \times 10^8$ s for T_{ISS} = 0.1 s and T_{1n} = 10 000 s.

IV. Discussion and conclusions

The original description of the TM mechanism proposed by Borghini and here analyzed in depth in terms of electron and nuclear polarization, polarization times and dynamics of the inverse spin temperatures has only a partial qualitative overlap with the experimental observations reported in the literature. As, for example, pointed out in Fig. 8 of ref. 18, the Borghini model overestimates the final values of P_n especially at the edges of the ESR line, leading to an unsatisfactory shape of the DNP spectrum (P_n *versus* ω_{MW}). Similarly, our computation of the model, even when the MW frequency is 3σ lower than ω_e (approx. 80 MHz with our choice of parameters) and consequently the electron population of the corresponding energy levels is very low, predicts a very high enhancement of the nuclear polarization which is quite unrealistic and – more importantly – not experimentally observed. Conversely, by relaxing either the constraint of a complete MW saturation or the constraint of a perfect electron–nucleus contact, lower P_n values and a sharper DNP spectrum are obtained (panels A in Fig. 2 and 3).

Furthermore, in the Borghini regime, the dependence of the efficiency of the polarization transfer on the microwave frequency (T_{pol} *vs.* ω_{MW}, panel C in Fig. 1) disagrees with the experimental observations reported for a sample of [1-13C]-pyruvic acid doped with 10 mM of trityl. In Fig. 5 of ref. 22 in fact Macholl *et al.* showed that T_{pol} is relatively short as long as ω_{MW} is set between the two values corresponding to the positive and negative maximum of nuclear polarization (DNP optimum frequencies) whilst becoming longer and longer on moving towards the edges of the ESR line. Remarkably, the correct qualitative behaviour of the polarization time is recovered under the assumptions underlying both regime II and regime III, as shown in panels B of Fig. 2 and 3. This type of dependence of T_{pol} on ω_{MW} seems not restricted to the reference sample and the magnetic field value considered so far, but rather general for DNP experiments performed at very low temperature. Similar behaviours have been reported in fact for a sample of [1-13C]-pyruvic acid doped with trityl 18.5 mM at 1.2 K and 4.64 T, corresponding to an electron Larmor frequency of 130 GHz (Fig. 3 in ref. 23), as well as for [1-13C]-labelled acetate doped with TEMPO 50 mM at both 3.35 T (Fig. 1 of ref. 24) and at 5 T (corresponding to $\omega_e \approx$ 140 GHz, Fig. 2 of ref. 24) at a

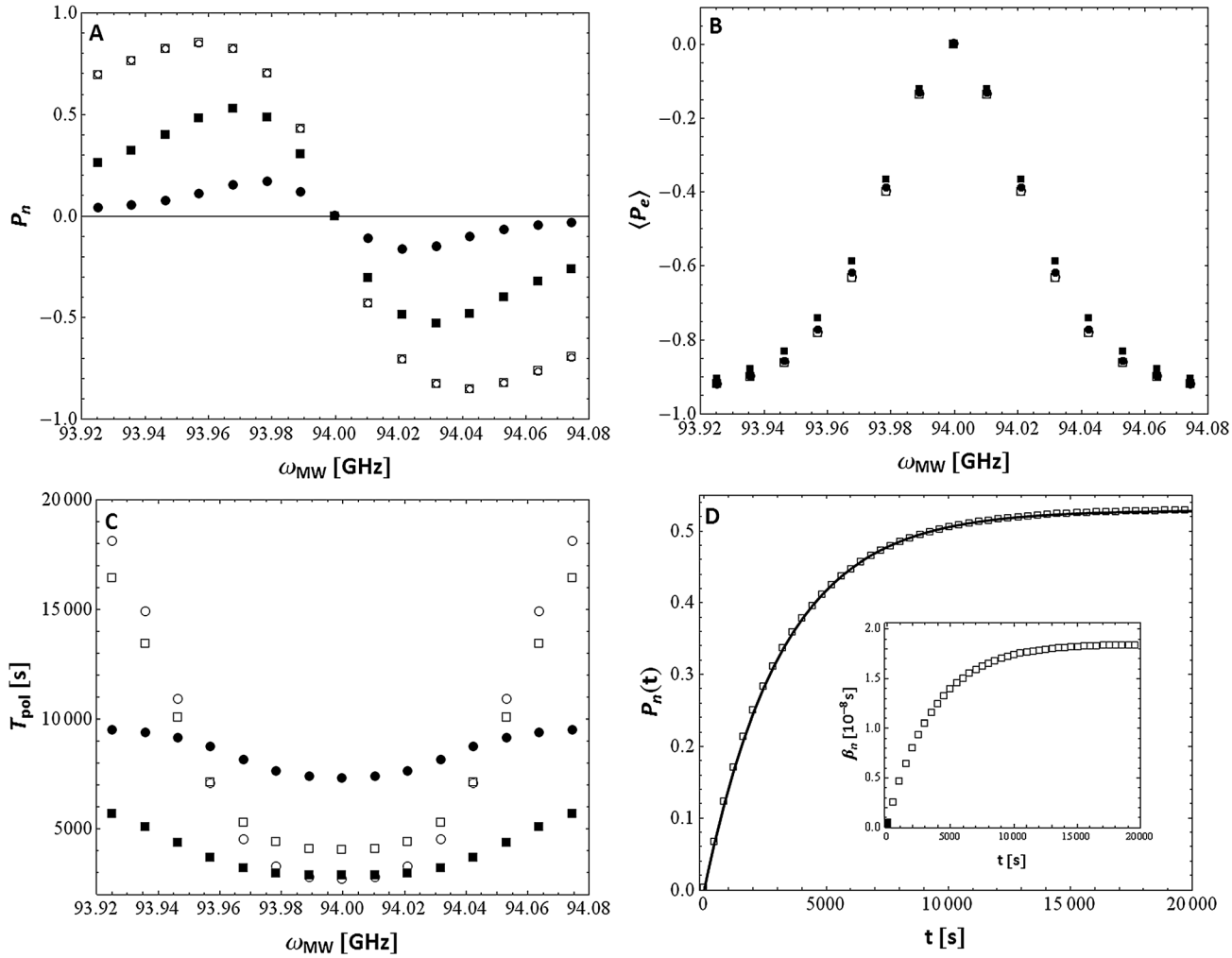

Fig. 3 Overview of nuclear and electron polarization in TM-DNP under the assumption defining regime III (T_{2e} = 0 s, T_{1MW} = 0 s, $T_{ISS} \neq 0$ s) at 3.35 T and 1.2 K, with N_n/N_e = 1000, T_{1e} = 1 s. Panel A: steady state nuclear polarization P_n as a function of the irradiating frequency ω_{MW} with T_{ISS} = 0.1 s (squares) or 1 s (circles) and in the absence of leakage (empty symbols) or with T_{1n} = 10 000 s (filled symbols). Panel B: average electron polarization $\langle P_e \rangle$ as a function of ω_{MW} with T_{ISS} = 0.1 s (squares) or 1 s (circles) and in the absence of leakage (empty symbols) or with T_{1n} = 10 000 s (filled symbols). Panel C: nuclear polarization time T_{pol} as a function of ω_{MW} with T_{ISS} = 0.1 s (squares) or 1 s (circles) and in the absence of leakage (empty symbols) or with T_{1n} = 10 000 s (filled symbols). Values represented with empty circles are scaled of a factor of $\frac{1}{10}$. Panel D: nuclear polarization build up curves $P_n(t)$ (squares) at $\omega_{MW,opt}$, T_{ISS} = 0.1 s and T_{1n} = 10 000 s. The solid line represents the best fit to an exponential function, while the inset displays the corresponding growth of the inverse temperature $\beta_n(t)$.

temperature of 1.2 K. The robustness of the predictions of the model analyzed here against magnetic field strength has been verified for both regime II (data not shown) and regime III (Fig. 4) by repeating the computation for our reference sample at higher field (parameters were set as follows, according to ref. 23: B_0 = 4.64 T, T = 1.2 K, T_{1e} = 1 s, $\Delta\omega_e$ = 63 MHz). The extension of our calculations to a model representing different radicals and eventually higher temperatures, for comparison with the experimental observations achieved under such conditions,[24–27] will be performed in a next dedicated study.

As long as only the nuclear parameters (P_n and T_{pol}) are considered, regimes II and III are both in qualitative agreement with the experimental observations and nearly superimposable.[22–24] Actually the two regimes are very different, as can be understood from panels B and D of Fig. 2 and 3. For limited MW power and T_{ISS} = 0, the nuclear system and the electron system share always the same inverse temperature, generally lower than the achieved β in the case of full saturation. In fact, as shown in panel B of Fig. 2, $\langle P_e \rangle$ tends to the frequency-independent equilibrium value P_0 when T_{1MW} increases, as the competition between the MW pumping and the electron spin–lattice relaxation unbalances the steady state towards the Boltzmann equilibrium. The electron system being weakly affected by MW irradiation, it is not anymore a forceful source of polarization for nuclei.

On the other hand, in the case of finite electron–nucleus contact and T_{1MW} = 0, the electron system under the effect of the saturating MW pumping reaches in a short time a *quasi*-stationary polarization profile, characterized by an inverse temperature β_e that slowly evolves while cooling the nuclear reservoir. In the absence of leakage the nuclear system sees

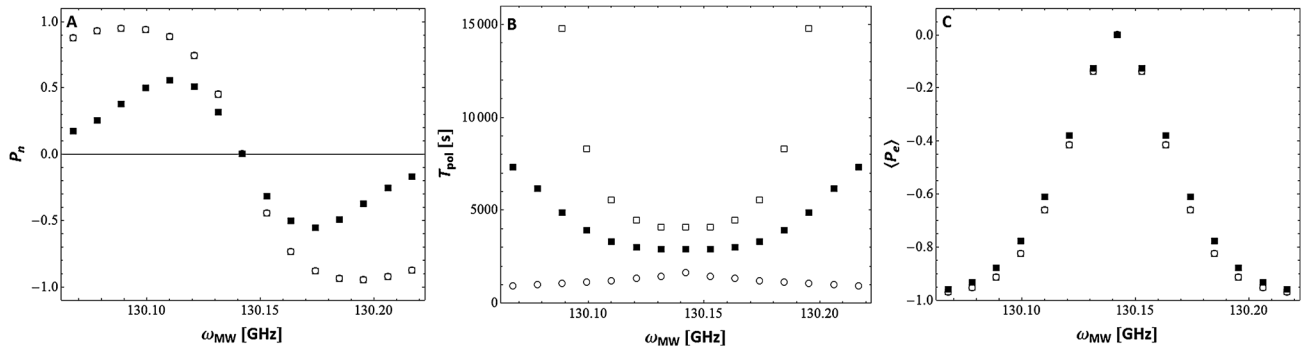

Fig. 4 Steady state nuclear polarization (panel A), nuclear polarization time (panel B) and steady state electron polarization (panel C) as a function of the microwave frequency at B_0 = 4.64 T and T = 1.2 K in the Borghini regime (empty circle) and in the finite electron nucleus contact regime (T_{1SS} = 0.1 s, without leakage (empty squares) and with T_{1n} = 10 000 s (filled squares)). Remaining parameters are set as follows $\delta\omega_e$ = 63 MHz, T_{1e} = 1 s, $T_{1n} = \infty$, N_n/N_e = 1000, δn_p = 3, N_p = 15.

only the pre-thermalized electron reservoir and, with a characteristic time dependent on the contact ratio $1/T_{1SS}$ reaches a final inverse temperature $\beta_n = \beta_e$. In the presence of leakage the nuclear reservoir is on one side in thermal exchange with the electron system at β_e and, on the other side, with the lattice at $\beta_L \propto 1/T$. The final nuclear inverse temperature β_n is a trade-off value between β_e and β_L and, as well as nuclear build up time, depends on the two contact parameters T_{1SS} and T_{1n}.

In order to discriminate which scenario fits better with the experimental observations, data for the behaviour of electrons must be considered. A valid attempt to characterize the electron system was made by Ardenkjaer-Larsen and collaborators and it is reported in ref. 18 and 23. By measuring the shift of the ^{13}C resonance line (M_1) caused mainly by the dipolar fields associated to the polarized paramagnetic centres, the authors indirectly estimated the average electron polarization $\langle P_e \rangle$ according to ref. 11:

$$M_1 = \tfrac{2}{3}\pi\xi\gamma_e\gamma_n\hbar N_e\langle P_e\rangle \qquad (14)$$

where ξ is a coefficient which depends on the shape of the sample, γ_e is the electron gyromagnetic ratio, γ_n is the nuclear gyromagnetic ratio and N_e is the number of electrons per unit volume.

In particular, in ref. 23 (Fig. 4–6) the dependence of the nuclear shift, and thus indirectly of $\langle P_e \rangle$, on the MW frequency and power was measured.[28]

The average electron polarization $\langle P_e \rangle$ at a fixed MW power (Fig. 5 and 6 of ref. 23) was found to depend on ω_{MW} with a behaviour similar to that reported in panel B of Fig. 1–3, where the degree of electron saturation is higher for $\omega_{MW} = \omega_e - \delta\omega$ and lower when moving towards the edges of the ESR line and, as expected, when the MW power is reduced. It is worth noting that M_1 increases rapidly at low microwave power and then reaches a plateau for power on the order of 40–60 mW. For a direct comparison of experimental (Fig. 4 of ref. 23) and computational data, the dependence of simulated levels of P_n and $\langle P_e \rangle$ as a function of the MW power, expressed by T_{1MW}, for different values of ω_{MW} is reported in Fig. 5. The same qualitative behaviour is obtained in experimental and calculated data. In numerical simulations the plateau is reached for $T_{1MW} \leq 0.05$–0.1 s, whereas experimentally a plateau of M_1 is reached above a few tens of mW. Such values are lower than the power level commonly used in DNP experiments at low temperature ($T \approx 1.2$ K), thus suggesting that the assumption of full saturation is more appropriate than the hypothesis of partial saturation in interpreting DNP results collected on trityl

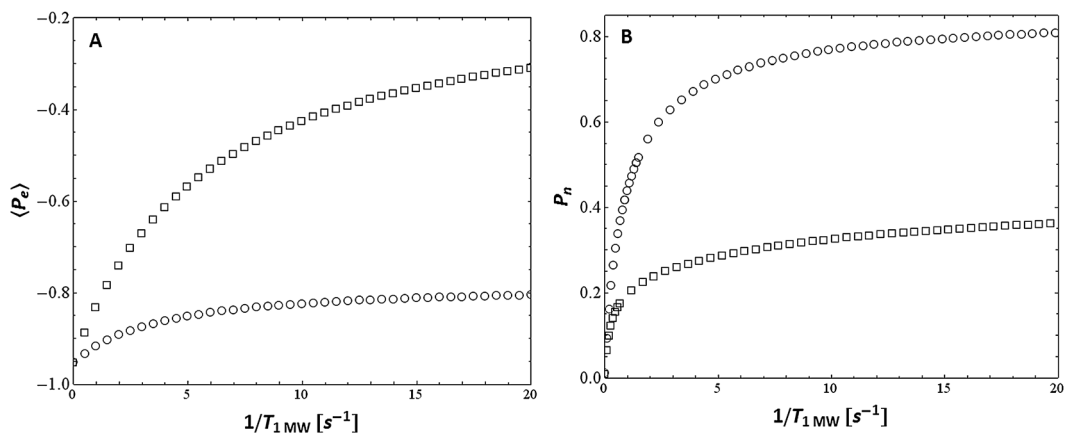

Fig. 5 Steady state polarization of the electron (panel A) and nuclear (panel B) spin systems as a function of the microwave power, expressed by the parameter T_{1MW}, for $\omega_{MW} = \omega_{MW,opt}$ (circles) and $\omega_{MW} = \omega_e - \delta\omega$ (squares). Remaining parameters are set as follows: T_{2e} = 0 s, T_{1SS} = 0, T_{1e} = 1 s, $T_{1n} = \infty$, N_n/N_e = 1000, δn_p = 3, N_p = 15.

doped samples in this temperature range. In ref. 19, Jannin *et al.* argued that the increase of the microwave power could lead, in the TEMPO doped sample considered, to a heating of the thermal bath which competes with the polarizing action of the MW themselves, affecting the equilibrium nuclear polarization and ending up in lower steady state P_n values. Such an argument cannot be extended to explain the observations on trityl doped samples, as the heating effect would also affect the equilibrium electron polarization, contributing positively to the total saturation of the ESR line. In that case, $\langle P_e \rangle$ should go to zero upon increasing the MW power ($1/\beta_e \rightarrow \infty$), instead of going to the low temperature plateau observed in ref. 23. Thus, the assumption of partial MW saturation, although successful in improving the description of DNP from the nuclear point of view, shows an intrinsic weakness in accounting for the electron behaviour of trityl doped samples (different conclusions may apply to DNP samples doped with different radicals, such as TEMPO, provided that $\langle P_e \rangle \rightarrow 0$ upon increasing the irradiation power). The model of finite electron–nucleus contact on the other hand, has similar capability in describing the nuclear system, but without explicitly contradicting the experimental behaviour of electrons. Overall, given the low temperature DNP experimental data available so far on the target compound considered here, relaxing the condition $T_{ISS} = 0$ appears more promising than removing the saturation condition $T_{1MW} = 0$.

An elegant experimental test for better judging the physical meaningfulness of regimes II and III would consist in measuring the electron polarization profiles $f_i P_{e,i}(\omega_{MW})$. The expected trends for the two regimes are shown in Fig. 6 for $\omega_{MW} = \omega_{MW,opt}$ (panels A and C) and for $\omega_{MW} = \omega_e - \delta\omega$ (panels B and D) and described by eqn (2): under the assumption of regime II $\beta_e = \beta_n$ and no packets are fully saturated, whereas in regime III in the absence of leakage $\beta_e \neq \beta_n$ and the irradiated packet is characterized by $P_{e,0} = 0$. Especially when ω_{MW} is set close to ω_e the electron profile of the two regimes is considerably different.

In summary we have presented the articulated picture of thermal mixing DNP generated by the five parameter model introduced in ref. 20, in the limit where $T_{2e} = 0$. Three cases in particular have been discussed in detail: the Borghini regime, characterized by a strong saturation of the ESR line and by a perfect contact between electrons and nuclei (T_{1MW} and $T_{ISS} = 0$), the regime of partial saturation of the ESR line ($T_{1MW} \neq 0$ and $T_{ISS} = 0$) and the regime of finite electron–nucleus contact ($T_{1MW} = 0$ and $T_{ISS} \neq 0$). The former regime has been shown to be less accurate in accounting for the available experimental observations, whereas the latter two are both capable of properly capturing more features of the nuclear spin dynamics, whilst predicting different behaviour for the electron system. Additional dedicated experiments would be desirable in order

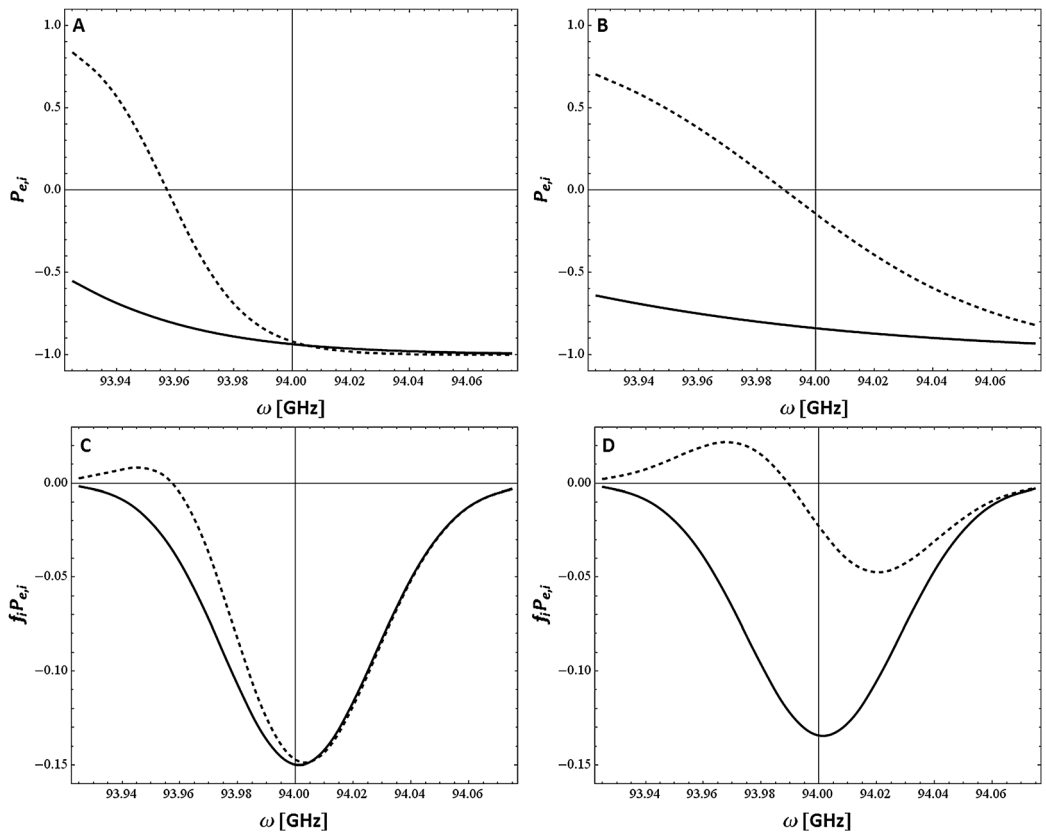

Fig. 6 Steady state electron polarization $P_{e,i}(t \rightarrow \infty)$ as a function of the electron frequency ω in the regime of partial saturation ($T_{1MW} = 1$ s, solid line) and of non-perfect electron–nucleus contact ($T_{ISS} = 1$ s, dashed line) for $\omega_{MW} = \omega_{MW,opt}$ (panel A) and for $\omega_{MW} = \omega_e - \delta\omega$ (panel B). Weighted electron polarization $f_i P_{e,i}(t \rightarrow \infty)$ as a function of the electron frequency ω in the regime of partial saturation ($T_{1MW} = 1$ s, solid line) and of non-perfect electron–nucleus contact ($T_{ISS} = 1$ s, dashed line) for $\omega_{MW} = \omega_{MW,opt}$ (panel C) and for $\omega_{MW} = \omega_e - \delta\omega$ (panel D). Remaining parameters are set as follows: $T_{2e} = 0$ s, $T_{1e} = 1$ s, $T_{1n} = \infty$, $N_n/N_e = 1000$, $\delta n_p = 3$, $N_p = 15$.

to clarify which of the two predictions gives a better picture of the physical reality, although the finite electron–nucleus contact regime looks more consistent than partial saturation in describing the behaviour of trityl doped samples on varying the MW irradiation power.

The theoretical picture provided in this work cannot capture by definition those polarization phenomena driven by the solid effect or by the cross effect. Moreover it is still unable to describe some facts observed in experiments where the thermal mixing mechanism is expected to dominate, such as the inverse dependence of the nuclear steady state polarization on electron concentration, observed systematically when the ratio N_e/N_n exceeds a certain value. The statistical approach introduced in ref. 20 however, can be extended to explore regimes with limited efficiency of the electron–electron interaction or, in other words, with limited thermal contact between different electronic packets. Moreover, the approach is flexible enough to allow the introduction of additional interaction terms. By exploiting these residual opportunities, we are confident that also the still unexplained behaviours will find suitable interpretation within the general framework of thermal mixing.

Appendix A: spin temperature in the thermal mixing regime

Abragam and Goldman[11] gave a description of TM DNP based on the separation between electron Zeeman and non-Zeeman contributions in the magnetic Hamiltonian of the system.

Starting from such Hamiltonian one may derive the energy of a single electron spin S_i (belonging to packet i) associated to its two possible states: *up* ($\uparrow$) of energy $E_i^{\uparrow} = \hbar/2(\omega_e - \Delta_i)$ and *down* ($\downarrow$), $E_i^{\downarrow} = -\hbar/2(\omega_e - \Delta_i)$. When MW is off, the system is at thermal equilibrium with the lattice, at an inverse temperature $\beta_L = \hbar/(2k_BT)$ (where k_B is the Boltzmann constant) and the probability for the spin S^i to be in the state *up* is given by the Boltzmann weight:

$$p_i^{\uparrow} \propto \exp[-\beta_L(\omega_e - \Delta_i)].$$

When MW is on, the system is out of equilibrium. If now the existence of a unique temperature among the different packets is postulated as in ref. 11, the probability $p_i^{\uparrow}$ can be expressed in terms of a generalized Boltzmann weight:

$$p_i^{\uparrow} \propto \exp\left[-\left(\frac{\hbar\omega_e}{2k_BT_\alpha} - \frac{\hbar\Delta_i}{2k_BT_\beta}\right)\right] = \exp[-(\alpha\omega_e - \beta\Delta_i)]$$

where the two parameters $\alpha = \hbar/(2k_BT_\alpha)$ and $\beta = \hbar/(2k_BT_\beta)$ are normally referred to as Zeeman and non-Zeeman inverse temperature respectively. The polarization of the spin S^i can be then written as:

$$P_i = \frac{p_i^{\uparrow} - p_i^{\downarrow}}{p_i^{\uparrow} + p_i^{\downarrow}} = -\tanh[\alpha\omega_e - \beta\Delta_i].$$

The same expression can be derived by observing that, whenever a process much faster than the other events ruling the system exists, the detailed balance for such a process must be satisfied at any point in time. In all the TM scenarios considered in this work, the 'spectral diffusion' mechanism depicted here below

$$\underset{\omega_{i-\delta}}{\downarrow}\ \underset{\omega_i}{\uparrow}\ \underset{\omega_j}{\uparrow}\ \underset{\omega_{j+\delta}}{\downarrow} \quad \underset{T_{2e}}{\rightleftharpoons} \quad \underset{\omega_{i-\delta}}{\uparrow}\ \underset{\omega_i}{\downarrow}\ \underset{\omega_j}{\downarrow}\ \underset{\omega_{j+\delta}}{\uparrow}$$

has been always assumed to be a fast process. Its corresponding detailed balance condition can be written in terms of the fraction of electrons *up* – $P_{e,i}^{+}(t)$ – and of the fraction of electrons *down* – $P_{e,i}^{-}(t)$ – at time t:

$$\frac{P_{e,i-\delta}^{+}(t)P_{e,i}^{-}(t)}{P_{e,i-\delta}^{-}(t)P_{e,i}^{+}(t)} = \frac{P_{e,j}^{+}(t)P_{e,j+\delta}^{-}(t)}{P_{e,j}^{-}(t)P_{e,j+\delta}^{+}(t)}.$$

Then, by using the relation

$$P_{e,i}^{+}(t) = \frac{1 + P_{e,i}(t)}{2}, \quad P_{e,i}^{-}(t) = \frac{1 - P_{e,i}(t)}{2}$$

one comes to an equation for the electron polarization

$$\frac{(1 - P_{e,i})(1 + P_{e,i-\delta})}{(1 + P_{e,i})(1 - P_{e,i-\delta})} = \frac{(1 + P_{e,j})(1 - P_{e,j+\delta})}{(1 - P_{e,j})(1 + P_{e,j+\delta})}$$

which is satisfied if

$$P_{e,i}(t) = \tanh[\beta_e(t)(\Delta_i - c(t))],$$

qed.

Repeating the same procedure for the ISS process one obtains the following equation for the nuclear polarization:

$$P_n(t) = \frac{P_{e,i}(t) - P_{e,i+\delta n_p}(t)}{1 - P_{e,i+\delta n_p}(t)P_{e,i}(t)} \tag{A1}$$

which, being $P_{e,i}(t) = \tanh[\beta(t)(\Delta_i - c(t))]$, can be rewritten as:

$$P_n(t) = \tanh[\beta(t)\delta n_p]. \tag{A2}$$

Eqn (A2), valid when T_{ISS} is as fast as spectral diffusion, defines the existence of a unique common temperature between the nuclear spin system and the electron non-Zeeman reservoir.

Appendix B: electron and nuclear spin dynamics

The numerical procedure described in the main text to evaluate $P_{e,i}(t)$ and $P_n(t)$, when all the processes but the spectral diffusion have a finite transition rate, has been conveniently adapted for the three regimes considered. The strategy consists in using conservation laws to manage all mechanisms assumed to be infinitely efficient, while computing rate equations only for processes with a finite rate.

1. Regime I: 'Borghini' (T_{ISS} and $T_{1MW} \to 0$)

Rate equations are used to account only for the effect of the electron and nuclear spin–lattice relaxation:

$$\begin{aligned} \frac{dP_{e,i}(t)}{dt} &= \frac{P_0 - P_{e,i}(t)}{T_{1e}} \\ \frac{dP_n(t)}{dt} &= \frac{P_{0n} - P_n(t)}{T_{1n}} \end{aligned} \tag{B1}$$

Fast processes (spectral diffusion, electron–nucleus contact and MW saturation) are accounted for by the conservation of

the total polarization (for variations induced by spectral diffusion or ISS) and of the total electron non-Zeeman plus nuclear Zeeman energies:

$$\sum f_i[P_{e,i}(t+\delta t) - P_{e,i}(t) - \delta_{i,i_0}\delta P^{MW}] = 0$$

$$\sum f_i\Delta_i\left[P_{e,i}(t+\delta t) - P_{e,i}(t)\right] - \frac{N_n}{N_e}\omega_n[P_n(t+\delta t) - P_n(t)] = 0$$

where δP^{MW} indicates the variation due to MW irradiation and the time step $\delta t \to 0$ being the characteristic time of the transitions T_{2e}, T_{ISS} and T_{1MW}. These equations are conveniently written as:

$$-\sum_{i\neq i_0} f_i\left[P_{e,i}(t+\delta t) - P_{e,i}(t)\right] = f_0\left[P_{e,0}(t+\delta t) - P_{e,0}(t) - \delta P^{MW}\right]$$

$$\sum_{i\neq i_0} f_i\Delta_i\left[P_{e,i}(t+\delta t) - P_{e,i}(t)\right] + f_0\Delta_0\left[P_{e,0}(t+\delta t) - P_{e,0}(t) - \delta P^{MW}\right] - \frac{N_n}{N_e}\omega_n[P_n(t+\delta t) - P_n(t)] = 0$$

so that, by means of simple algebra, the condition:

$$\sum f_i(\Delta_i - \Delta_0)\left[P_{e,i}(t+\delta t) - P_{e,i}(t)\right] - \frac{N_n}{N_e}\omega_n[P_n(t+\delta t) - P_n(t)] = 0 \quad \text{(B2)}$$

is obtained. By solving this equation one derives $\beta(t+\delta t)$ and computes $P_{e,i}(t+\delta t) = -\tanh[\beta(t+\delta t)(\Delta_i - \Delta_0)]$ and $P_n(t+\delta t) = \tanh[\beta(t+\delta t)\delta n_p]$.

It is interesting to study also the evolution of the inverse temperature $\beta(t)$ that in regime I, as demonstrated in the Appendix A, is the same for both the electron non-Zeeman and the nuclear Zeeman reservoirs: $\beta(t) = \beta_e(t) = \beta_n(t)$. Moreover, since full saturation imposes $c = \Delta_0$, $\beta(t)$ is the only unknown variable of the problem. Hence, by means of eqn (B2) and (B1), it is possible to describe analytically the time behaviour of $\beta(t)$. At a generic time $t + dt$, by assuming $\delta t \to 0$, eqn (B2) writes:

$$\sum f_i\left\{-\tanh[\beta(t+dt)(\Delta_i - \Delta_0)] - P_{e,i}(t+dt)\right\}(\Delta_i - \Delta_0) - \frac{N_n}{N_e}\omega_n[\tanh(\beta(t+dt)\omega_n) - P_n(t+dt)] = 0$$

Now, using eqn (B1) for replacing $P_{e,i}(t+dt)$ and $P_n(t+dt)$ one obtains:

$$\sum f_i\left\{-\tanh[\beta(t+dt)(\Delta_i - \Delta_0)] + \tanh[\beta(t)(\Delta_i - \Delta_0)]. - \frac{dt}{T_{1e}}P_0 - \tanh[\beta(t)(\Delta_i - \Delta_0)]\right\}(\Delta_i - \Delta_0) - \frac{N_n}{N_e}\omega_n[\tanh(\beta(t+dt)\omega_n) - \tanh(\beta(t)\omega_n)] = 0$$

Then, with the first order expansions:

$$\beta(t+dt) \approx \beta(t) + \beta'(t)\,dt$$

$$\tanh[\beta(t+dt)x] \approx \tanh[\beta(t)x] + \beta'(t)x\{1 - \tanh^2[\beta(t)x]\}$$

and some algebraic calculations, the following equation for $\beta(t)$ is achieved:

$$\beta'(t)\left\{\sum f_i(\Delta_i - \Delta_0)^2\left[1 - \tanh^2[\beta(t)(\Delta_i - \Delta_0)]\right]. + \frac{N_n}{N_e}\omega_n{}^2\left[1 - \tanh^2[\beta(t)\omega_n]\right]\right\} + \frac{1}{T_{1e}}\sum f_i(\Delta_i - \Delta_0)\{P_0 + \tanh[\beta(t)(\Delta_i - \Delta_0)]\} = 0 \quad \text{(B3)}$$

Eqn (B3) is conveniently rewritten as:

$$\beta'(t) = -\frac{\sum f_i(\Delta_i - \Delta_0)\tanh[\beta(t)(\Delta_i - \Delta_0)] - \Delta_0 P_0}{\frac{N_n}{N_e T_{1e}}\omega_n{}^2\left[1 - \tanh^2[\beta(t)\omega_n]\right]}, \quad \text{(B4)}$$

after neglecting with good approximation the term $\sum f_i(\Delta_i - \Delta_0)^2\,[1 - \tanh^2[\beta(t)(\Delta_i - \Delta_0)]]$.

Although no attempt to solve analytically eqn (B4) is made here, it is clear that the solution cannot be an exponential function, as already anticipated in the main text.

2. Regime II: partial MW saturation (T_{2e}, $T_{ISS} \to 0$)

The system of rate equations is used to describe the effect of partial MW saturation as well as electron and nuclear spin–lattice relaxation:

$$\frac{dP_{e,i}(t)}{dt} = \frac{P_0 - P_{e,i}(t)}{T_{1e}} - \delta_{i,i_0}\frac{P_{e,0}}{T_{1MW}}$$

$$\frac{dP_n(t)}{dt} = \frac{P_{0n} - P_n(t)}{T_{1n}}$$

whereas spectral diffusion and electron–nucleus interaction are accounted for by the following conservation laws:

$$\sum f_i[P_{e,i}(t+\delta t) - P_{e,i}(t)] = 0$$

$$\sum f_i\Delta_i\left[P_{e,i}(t+\delta t) - P_{e,i}(t)\right] - \frac{N_n}{N_e}\omega_n[P_n(t+\delta t) - P_n(t)] = 0$$

with $\delta t \to 0$ being the characteristic time of the transitions T_{2e} and T_{ISS}. By solving this system one obtains $\beta(t+\delta t)$ and $c(t+\delta t)$ and computes $P_{e,i}(t+\delta t) = -\tanh[\beta(t+\delta t)(\Delta_i - c(t))]$ and $P_n(t+\delta t) = \tanh[\beta(t+\delta t)\delta n_p]$.

3. Regime III: poor electron–nucleus contact (T_{2e} and $T_{1MW} \to 0$)

The system of rate equations takes into account the effect of the electron–nucleus contact and of the electron and nuclear spin–lattice relaxation:

$$\frac{dP_{e,i}(t)}{dt} = \frac{P_0 - P_{e,i}(t)}{T_{1e}} + \frac{f_{i-\delta n_p}\Pi_- + f_{i+\delta n_p}\Pi_+}{2T_{ISS}}$$

$$\frac{dP_n(t)}{dt} = \frac{P_{0n} - P_n(t)}{T_{1n}} - \frac{N_e}{2T_{ISS}N_n}\sum f_i f_{i+\delta n_p}\Pi_n$$

The effect of the other processes (spectral diffusion and full MW saturation) is accounted for by the conservation of the total polarization (when the variation is induced by spectral diffusion)

and of the total electron non-Zeeman plus nuclear Zeeman energies:

$$\sum f_i[P_{e,i}(t+\delta t) - P_{e,i}(t) - \delta_{i,i_0}\delta P^{MW}] = 0$$

$$\sum f_i\Delta_i[P_{e,i}(t+\delta t) - P_{e,i}(t)] = 0$$

where δP^{MW} indicates the variation due to MW irradiation and the time step $\delta t \to 0$ being the characteristic time of the transitions T_{2e} and T_{1MW}. These equations are conveniently written as:

$$-\sum_{i\neq i_0} f_i\left[P_{e,i}(t+\delta t) - P_{e,i}(t)\right] = f_0\left[P_{e,0}(t+\delta t) - P_{e,0}(t) - \delta P^{MW}\right]$$

$$\sum_{i\neq i_0} f_i\Delta_i\left[P_{e,i}(t+\delta t) - P_{e,i}(t)\right] + f_0\Delta_0\left[P_{e,0}(t+\delta t) - P_{e,i}(0) - \delta P^{MW}\right] = 0$$

so that, after simple algebraic calculations, the following condition is obtained:

$$\sum f_i(\Delta_i - \Delta_0)[P_{e,i}(t+\delta t) - P_{e,i}(t)] = 0,$$

that allows deriving $\beta(t+\delta t)$ and thus computing $P_{e,i}(t+\delta t) = -\tanh[\beta(t+\delta t)(\Delta_i - \Delta_0)]$.

Appendix C: dynamical behaviour of the electron average polarization

The evolution of the average electron polarization $\langle P_e\rangle$ in regimes II and III shows a peculiar behaviour characterized by two different time scales, as sketched in Fig. 7.

1. Partial MW saturation

In this regime, due to the hypothesis $T_{2e} = 0$ and $T_{ISS} = 0$, one has $P_{e,i}(t) = \tanh[\beta_e(t)(\Delta_i - c(t))]$ and $\beta_e(t) = \beta_n(t) = \beta(t)$. The evolution of $\langle P_e\rangle$ is determined both by $\beta(t)$ (panel D, Fig. 2) and $c(t)$.

At short times ($t \approx T_{1e}$) the inverse temperature β is determined by the large nuclear system for which $\beta_n(t=0) = \beta_L \approx 0$. When $T_{1MW} = 0$, the only solution is $c(t=0) = \Delta_0$ and consequently $P_{e,i}(t=0) = 0$, $\forall i$. For partial saturation ($T_{1MW} > 0$) the profile of $P_{e,i}$ becomes a flat function (corresponding to the condition $c(t=0) \to \infty$), which quickly evolves with a characteristic time T_{1e} towards an intermediate level between 0 and P_0, that can be calculated using the first equation of system (8):

$$P_{e,i} = P_0\frac{T_{1MW}}{f_0T_{1e} + T_{1MW}}.$$

At longer times ($t \approx T_{pol}$) the evolution of $\langle P_e\rangle$ is mainly due to $\beta(t)$ dynamics ($c(t)$ being approximately constant) and it is thus characterized by a time constant in the order of 10^3 s.

2. Poor electron–nucleus contact

The dynamics of both $\beta_e(t)$ and $\langle P_e(t)\rangle$ is characterized by two time scales: a first rapid component with a characteristic time in the order of T_{1e} and a second slow component with a characteristic time in the order of T_{pol}.

In this regime, due to the hypothesis $T_{2e} = 0$ and $T_{1MW} = 0$, one has $P_{e,i}(t) = \tanh[\beta_e(t)(\Delta_i - \Delta_0)]$, with $\beta_e(t) \neq \beta_n(t)$. Depending on the time scale considered, the system can be qualitatively depicted and β_e estimated accordingly.

- At very short times ($t \to 0$), being the contact between electrons and nuclei finite, the electron system is unaffected by the presence of the nuclear reservoir and reaches immediately the inverse temperature β_B predicted by Borghini and defined by eqn (B2) after setting $N_n = 0$.
- After this initial 'thermalization' phase, at times $t \approx T_{1e}$, the electron reservoir is on one side in contact with a thermal bath at temperature $1/\beta_B$ (determined by interaction with the lattice,

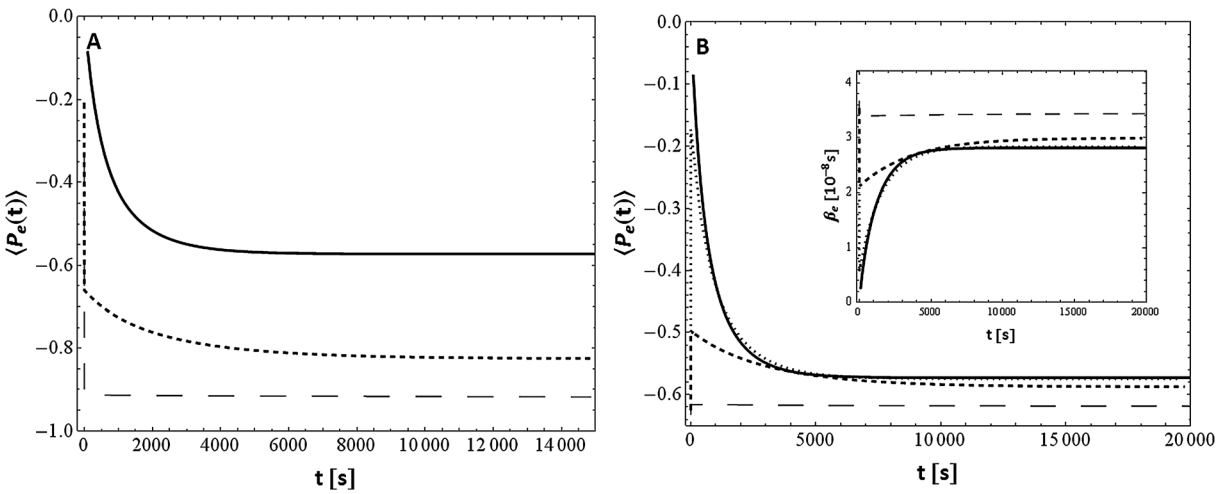

Fig. 7 Panel A: build up curve of the average electron polarization $\langle P_e(t)\rangle$ in the regime of partial saturation (regime II) for $T_{1MW} = 0$ s (Borghini limit, thick solid line), 0.1 s (small-dashed line) and 1 s (large-dashed line). Remaining parameters are set as follows: $T_{1e} = 1$ s, $T_{1n} = \infty$, $N_n/N_e = 1000$, $i_0 = 4$, $\delta n_p = 3$, $N_p = 15$. Panel B: build up curve of the average electron polarization $\langle P_e(t)\rangle$ and of the inverse electron spin temperature $\beta_e(t)$ (inset) in the regime of poor electron–nucleus contact for $T_{ISS} = 0$ s (Borghini limit, thick solid line), 0.01 s (dotted line), 0.1 s (small-dashed line) and 1 s (large-dashed line). Remaining parameters are set as follows: $T_{1e} = 1$ s, $T_{1n} = 10\,000$ s, $N_n/N_e = 1000$, $i_0 = 5$, $\delta n_p = 3$, $N_p = 15$.

by spectral diffusion and by the highly effective MWs), while feeling on the other side the nuclear ensemble having an initial temperature $\beta_n = \beta_L \approx 0$. Thus, on a time scale of a few T_{1e}, the inverse temperature β_e moves towards a target value between β_B and β_L, depending on the strength of the two contact times T_{1e} and T_{ISS}. When the electron–nucleus contact is poorly efficient $\beta_e \rightarrow \beta_B$; conversely $\beta_e \rightarrow \beta_L \approx 0$ for strong electron–nucleus contact.

• At large times ($t \approx T_{pol}$), $\beta_n(t)$ evolves from β_L towards its final steady state β_n and $\beta_e(t)$ evolves as well, reaching an intermediate value between β_n and β_B.

In summary, as long as the electron–nucleus contact is poorly efficient, the electron inverse temperature β_e is only slightly affected by the nuclear reservoir and it is thus seen by the latter as a constant value equal to β_B. As discussed in Sections II and IV this behaviour leads straightforwardly to an exponential build up curve for nuclear polarization.

Acknowledgements

This study has been supported in part by Regione Piemonte (POR FESR 2007/2013, line I.1.1), by the COST Action TD1103 (European Network for Hyperpolarization Physics and Methodology in NMR and MRI) and by ANR grant 09-BLAN-0097-02.

References

1 J. H. Ardenkjaer-Larsen, B. Fridlund, A. Gram, G. Hansson, L. Hansson, M. H. Lerche, R. Servin, M. Thaning and K. Golman, *Proc. Natl. Acad. Sci. U. S. A.*, 2003, **100**, 10158.
2 D. Hall, D. Maus, G. Gerfen, S. Inati, L. Becerra, F. Dahlquist and R. Griffin, *Science*, 1997, **276**, 930.
3 M. Rosay, J. Lansing, K. Haddad, W. Bachovchin, J. Herzfeld, R. Temkin and R. Griffin, *J. Am. Chem. Soc.*, 2003, **125**, 13626.
4 K. Golman, R. int Zandt, M. Lerche, R. Pehrson and J. H. Ardenkjaer-Larsen, *Cancer Res.*, 2006, **22**, 66.
5 S. E. Day, M. I. Kettunen, F. A. Gallagher, D. Hu, M. Lerche, J. Wolber, K. Golman, J. H. Ardenkjaer-Larsen and K. M. Brindle, *Nat. Med.*, 2007, **13**, 1382.
6 J. Kurhanewicz, D. B. Vigneron, K. Brindle, E. Y. Chekmenev, A. Comment, C. H. Cunningham, R. J. DeBerardinis, G. G. Green, M. O. Leach, S. S. Rajan, R. R. Rizi, B. D. Ross, W. S. Warren and C. R. Malloy, *Neoplasia*, 2011, **13**, 81.
7 Y. Hovav, A. Feintuch and S. Vega, *J. Chem. Phys.*, 2011, **134**, 074509.
8 A. Karabanov, A. van der Drift, L. J. Edwards, I. Kuprovb and W. Köckenberger, *Phys. Chem. Chem. Phys.*, 2012, **14**, 2658.
9 Y. Hovav, A. Feintuch and S. Vega, *J. Magn. Reson.*, 2012, **214**, 29.
10 J. R. Khutsishvili, *Sov. Phys. Usp.*, 1966, **8**, 747.
11 A. Abragam and M. Goldman, *Nuclear magnetism: order and disorder*, Clarendron Press, Oxford, 1982.
12 A. V. Kessenikh, V. I. Lushchikov, A. A. Manekov and Y. V. Taran, *Sov. Phys.*, 1963, **5**, 321.
13 A. V. Kessenikh, A. A. Manekov and G. I. Pyatnitskii, *Sov. Phys.*, 1964, **6**, 641.
14 C. F. Hwang and D. A. Hill, *Phys. Rev. Lett.*, 1967, **18**, 110.
15 C. F. Hwang and D. A. Hill, *Phys. Rev. Lett.*, 1967, **19**, 1011.
16 M. Borghini, *Phys. Rev. Lett.*, 1968, **20**, 419.
17 W. T. Wenckebach, T. J. B. Swaneburg and N. J. Poulis, *Phys. Rep.*, 1974, **14**, 181.
18 J. H. Ardenkjaer-Larsen, S. Macholl and H. Johannesson, *Appl. Magn. Reson.*, 2008, **34**, 509.
19 S. Jannin, A. Comment and J. J. van der Klink, *Appl. Magn. Reson.*, 2012, **43**, 59.
20 S. Colombo Serra, A. Rosso and F. Tedoldi, *Phys. Chem. Chem. Phys.*, 2012, **14**, 13299.
21 The main contribution to the line broadening is assumed to be single ion anisotropy (*i.e.* spreading of *g*-factors), while the influence of dipolar electron–electron interaction on the broadening is neglected. As far as a sample doped with 15 mM of trityl radical is concerned, the typical ESR line width at $T = 1.2$ K and $B_0 = 3.35$ T is about 63 MHz, whereas the electron–electron dipolar interaction is about 2 MHz. Despite the electron dipolar interaction brings a negligible contribution to the line width, it plays an important role as a source of spectral diffusion between different spin packets.
22 S. Macholl, H. Johannesson and J. H. Ardenkjaer-Larsen, *Phys. Chem. Chem. Phys.*, 2010, **12**, 5804.
23 H. Johannesson, S. Macholl and J. H. Ardenkjaer-Larsen, *J. Magn. Reson.*, 2009, **197**, 167.
24 S. Jannin, A. Comment, F. Kurdzesau, J. A. Konter, P. Haute, B. van den Brandt and J. J. van der Klink, *J. Chem. Phys.*, 2008, **128**, 241102.
25 L. Becerra, G. Gerfen, R. Temkin, D. Singel and R. Griffin, *Phys. Rev. Lett.*, 1993, **71**, 3561.
26 V. Bajaj, C. Farrar, M. Hornstein, I. Mastovsky, J. Vieregg, J. Bryant, B. Elena, K. Kreischer, R. Temkin and R. Griffin, *J. Magn. Reson.*, 2003, **160**, 85.
27 A. B. Barnes, E. Markhasin, E. Daviso, v. K. Michaelis, E. A. Nanni, S. K. Jawla, E. L. Mena, R. DeRocher, A. Thakkar, P. P. Woskov, J. Herzfeld, R. Temkin and R. Griffin, *J. Magn. Reson.*, 2012, **224**, 1.
28 The experiments in ref. 23 have been performed at 4.64 T while the results of our calculation presented in Section III have been obtained at 3.35 T. We have however repeated the calculation of $\langle P_e \rangle$ at 4.64 T and found that its qualitative behaviour is not affected by the intensity of B_0, as shown in Fig. 4, panel C.

